Submitted to *Meteorol. Z.*, Manuscript No. **A–0726**

Instantaneous fluctuations of temperature and moisture in the upper troposphere and tropopause region.

Part 1: Probability densities and their variability

Klaus Gierens [1,*], Regina Kohlhepp [1], Nikolai Dotzek [1],
and Herman G. Smit [2]

[1] DLR–Institut für Physik der Atmosphäre,
Oberpfaffenhofen, 82234 Wessling, Germany

[2] FZJ–Institut für Chemie und Dynamik der Geosphäre, ICG-II
Forschungszentrum Jülich, Leo–Brandt–Str., 52429 Jülich, Germany

2nd revised version

[*] *Corresponding Author:* Dr. Klaus Gierens, DLR–Institut für Physik der Atmosphäre, Oberpfaffenhofen, 82234 Wessling, Germany. Tel: +49–8153–28–2541, Fax: +49–8153–28–1841, eMail: klaus.gierens@dlr.de, http://www.pa.op.dlr.de/ pa1x/

Abstract

Using nine years (1995–2003) of MOZAIC temperature and humidity data, we analyse the statistics of instantaneous fluctuations of temperature, relative and absolute humidity with various spatial resolutions. We determine the probability density functions (p.d.f.s), their low order moments up to kurtosis, and study how these quantities vary with spatial resolution and with the background mean relative humidity. Seasonal and geographical variations are considered. Bivariate distributions of joint fluctuations of temperature and relative humidity are presented as well. These investigations are thought to provide an observational basis for the validation of statistical cloud schemes for large–scale models. For instance, we can show that temperature fluctuations cannot be neglected in such a scheme and that the bivariate distributions of simultaneous fluctuations of temperature and humidity have to be taken into account.

Keywords: Fluctuations; Tropopause; Statistical Modelling

Instantane Fluktuationen von Temperatur und Feuchte in der oberen Troposphäre und der Tropopausenregion. Teil 1: Wahrscheinlichkeitsdichten und deren Variabilität

Zusammenfassung

Instantane Fluktuationen von Temperatur und relativer Feuchte auf verschiedenen räumlichen Skalen werden mit Hilfe von MOZAIC Daten aus neun Jahren (1995–2003) untersucht. Wahrscheinlichkeitsdichteverteilungen werden bestimmt, deren Momente bis zur vierten Ordnung (d.h. Varianz, Schiefe, und Wölbungsmaß), sowie die Abhängigkeit dieser Größen von der räumlichen Auflösung und der mittleren relativen Feuchte. Saisonale und geographische Unterschiede werden betrachtet. Bivariate Verteilungen gemeinsamer Fluktuationen von Temperatur und relativer Feuchte werden ebenfalls präsentiert. Diese Untersuchung soll die Datengrundlage für Validationszwecke von statistischen Wolkenschemata für groß–skalige Modelle liefern. Wir zeigen beispielsweise, dass in einem solchen Schema Temperaturfluktuationen nicht vernachlässigt werden können, und dass man die bivariaten Verteilungen gleichzeitiger Fluktuationen von Temperatur und Feuchte verwenden muss.

Schlüsselwörter: Fluktuationen; Tropopause; Statistische Modellierung

1 Introduction

In order to compute cloud formation and coverage, large–scale atmospheric models for weather prediction or climate simulation generally need to make assumptions on the probability density function (p.d.f.) of fluctuations of humidity (typically mixing ratio of water in all its phases) and temperature with respect to their mean values in the grid cells. Models of the current generation generally use an *ad hoc* assumption on the distribution of these fluctuations that is based on the principle of mathematical simplicity to allow the computation the evolution of the distribution. However, these distributions are rarely checked against actual fluctuation data, since these are difficult to obtain.

GIERENS etal. (1997) used one year of MOZAIC data (Measurement of ozone, water vapour, carbon monoxide and nitrogen oxides by Airbus in–service aircraft, see MARENCO etal., 1998; BORTZ etal., 2006) to model a bivariate p.d.f. of simultaneous fluctuations of temperature and relative humidity in T42 resolution ($\simeq$300 km). Their objective was to derive a parameterisation for the fractional coverage of persistent condensation trails (contrails) in large–scale models. The idea is, that in a certain part of the $\{T, RH_i\}$ phase space, formation and persistence of contrails is locally possible, but not in the remaining part of the phase space. Thus, the contrail coverage in a grid cell is that portion of the p.d.f. of the fluctuations that is contained in the respective part of the phase space. This is also called the overlap integral.

An analogous strategy generally works for cloud formation. While the boundary between these two parts of the phase space is simply the saturation line for water clouds (i.e. RH over water equals 100%, independent of temperature), the corresponding boundary for ice clouds depends both on temperature and relative humidity over ice, and also on the ice–forming ability of the background aerosol. The threshold of relative humidity for ice formation increases with decreasing temperature and is generally much higher than 100%. For the prediction of cloud (both water and ice clouds) and contrail formation it is necessary to consider the bivariate p.d.f. of common temperature and humidity fluctuations because the relative humidity depends via the saturation vapour pressure on temperature. Hence, even when the threshold relative humidity is independent of temperature as for water clouds, temperature fluctuations alone can drive an air parcel over the cloud formation RH threshold.

MOZAIC data can be used for validation purposes, i.e. fluctuation distributions used in models can be checked against corresponding data from MOZAIC. One advantage of MOZAIC

is that we can use many years of data from thousands of flights, ensuring good statistics for our purpose. We have therefore started to analyse the fluctuations that can be obtained from that data base. In the following, we present in Sec. 2 the treatment of the MOZAIC data, and describe the statistical analysis of the scalar fluctuations, their dependence on spatial resolution, and their seasonal and geographical variation. Some technical and practical issues are discussed in Sec. 3, and results are summarised in Sec. 4. Further discussions on signs of intermittency (e. g. SORNETTE, 2004) in the p.d.f.s of the fluctuations and an apparent analogy of the MOZAIC p.d.f.s to small–scale turbulent Rayleigh–Bénard convection p.d.f.s. will be provided by Part 2 of our analysis (DOTZEK etal., 2006).

2 Statistical analyses of fluctuations

2.1 MOZAIC data

Within the MOZAIC programme the large scale distribution of water vapour is measured since August 1994 on board of five Airbus A340 aircraft during scheduled flights operated by civil airlines (MARENCO etal., 1998). The compact airborne sensing device used in MOZAIC for the measurement of relative humidity (capacitive sensor) and temperature (PT100–sensor) is described by HELTEN etal. (1998). The sensors are calibrated in the laboratory before and after 500 hours of flight operation. From the regular pre– and post flight calibration of each flown sensor typical 2σ–uncertainties of $\pm(5-10)\%$ relative humidity between 9 and 12 km altitude were derived (HELTEN etal., 1998). The in–flight performance of the MOZAIC–humidity device had been assessed by inter-comparison with reference instrumentation during dedicated aircraft missions (HELTEN etal., 1998, 1999) and confirmed the results yielded from pre– and post calibrations. The dynamical response time of the humidity sensor is about 1–2 minutes such that, at an aircraft speed of 250 m/s, the horizontal resolution is about 15–30 km while the vertical resolution is about 250–500 m. The temperature can be measured with an accuracy (systematic, but unknown error component) of about $\pm(0.5-0.7)$ K and a precision (random error) better than $\pm(0.1-0.2)$ K (HELTEN etal., 1998). Although the raw data are sampled every 4 s, the inertia of the humidity sensor makes it necessary to use the coarser resolution of $\Delta t = 1$ min which corresponds to $\Delta x \approx 15$ km spatial resolution. Fluctuations on scales smaller than a few times 15 km cannot be resolved.

We use MOZAIC temperature and humidity data from the pressure range 175–275 hPa gathered during nine complete years (1995–2003). Data with quality–control label "3" indicating doubtful quality have been discarded from the analysis. Hence, only records with reliable humidity value or indicating "too dry" for the sensor are retained for the analysis. In the selected pressure range the aircraft are in cruise, that is, the data come from quasi–stationary flight conditions and are essentially horizontally sampled (exceptions occur occasionally when aircraft change flight level).

Given the MOZAIC resolution Δx for the scalar fluctuations for temperature (δT), water vapour pressure (δe), and relative humidity over ice (δRH_i), statistical quantities of the data series can be computed. We use here the same procedure as of GIERENS etal. (1997) to compute the fluctuations. First, the globe is covered with a grid that is used also in large–scale models, here a Gaussian grid for spherical harmonics with triangular cut–off. If a flight path is long enough within one grid box (more than 8 min) we take all the measurements within that grid box, compute their average and the single deviations from that average. The latter are the instantaneous fluctuations of the respective quantity. They are collected for every flight and every grid box wherein the flight path allows a sufficient number of observations.

For the statistical description we use the first four moments of the distributions of the fluctuations. The mean value (the first moment) vanishes by definition, so all moments are automatically central moments. The second to fourth central moments (standard deviation σ, skewness S and kurtosis W) of a discrete scalar quantity ξ measured at times t_n or locations x_n are conventionally defined as follows:

$$\sigma^2(\xi_1,\ldots,\xi_N) = \frac{1}{N-1}\sum_{n=1}^{N}\xi_n^2 \quad , \tag{1}$$

$$S(\xi_1,\ldots,\xi_N) = \frac{1}{N}\sum_{n=1}^{N}\left(\frac{\xi_n}{\sigma}\right)^3 \quad , \tag{2}$$

$$W(\xi_1,\ldots,\xi_N) = \left[\frac{1}{N}\sum_{n=1}^{N}\left(\frac{\xi_n}{\sigma}\right)^4\right] - 3 \quad . \tag{3}$$

In the following we describe the shape of the p.d.f.s often as concave or convex. For clarification: convex means that the function either increases more steeply than linearly or decreases less steeply than linearly (in other words, its second derivative is positive); for a concave shape it is vice versa.

The p.d.f.s are generally shown as histograms. For their construction we have binned fluctuations of relative humidity in classes 0.5% wide, those of vapour partial pressure in 0.1 Pa classes, and those of temperature in classes of 0.1 K width.

2.2 Distributions of δT, δe, and δRH_i in T42 resolution

We first consider distributions of temperature, moisture, and relative humidity fluctuations in T42 resolution. In T42 the globe is divided into 128×64 (longitude × latitude) grid boxes, that is, on the equator the spatial scale is about 300×300 km^2. We show all distributions in semi–logarithmic coordinates in order to make the distribution tails more discernible.

Fig. 1a shows the distribution of instantaneous fluctuations of temperature, δT, in two layers in the tropopause region, from 275 to 225 hPa and from 225 to 175 hPa, corresponding to the approximate altitude levels $z = 9.8$ to 11 km and 11 to 12.5 km, respectively. There are two remarkable features in these distributions: First, they are peaked at their mean value ($\delta T = 0$) and second, they are by no means Gaussian. Instead, the distribution tails conform better to exponentials (so–called Laplace distributions). However, there is a slight tendency of an S–shape on both tails of the distributions (i.e. concave–convex on the lower tail, and convex–concave on the upper tail). In the following, we will call this an ogival shape[1], not to be confused here with the frequent use of the word ogive for the cumulative distribution function (c.d.f.).

The distribution of the fluctuations of water vapour partial pressure, δe, is shown in Fig. 1b for the two pressure ranges, $275 \geq p \geq 225$ hPa and $225 \geq p \geq 175$ hPa. These distributions are sharply peaked at their mean value, even more than the fluctuations of temperature. They are neither Gaussian nor exponential, nor do they have an ogival shape. Instead, both tails are convex.

We have also evaluated the relative fluctuations $\delta e/e$, in view of the exponential profile of water vapour concentration in the atmosphere (not shown). Apart from the cut–off at -1, the distribution displays the same features as those of the absolute fluctuations of e, viz. sharply peaked at zero fluctuation, non–Gaussian shape, and convex tails.

The distribution of fluctuations of relative humidity with respect to ice, δRH_i, is shown in Fig. 1c. It is sharply peaked, non–Gaussian and non–exponential. The ogival shape is very

[1]The ogival arch, a pointed arch, is a feature of Gothic cathedrals. It has been introduced in northern France in the 13th century.

pronounced in this distribution. It can be explained as the result of a (weighted) convolution of the distributions of δT and δe, since both fluctuations of temperature and vapour pressure contribute to fluctuations of relative humidity (GIERENS etal., 1997).

As an overview of the results obtained so far for T42 resolution, we present in Table 1 the statistical description of the analysed data, i.e. the low order moments. Although not clearly apparent from the figures, our data have a certain degree of skewness, even the fluctuations of temperature and relative humidity. The kurtosis in our data is quite considerable, which is a property of sharply peaked distributions. Since the number of data records in our analysis is very large (about 5 million), all deviations from zero of skewness and kurtosis are statistically significant.

Table 1 also shows the low order moments obtained for northern winter (DJF) and summer (JJA) seasons. It can be seen that the annual variation of the fluctuation statistics for temperature, relative humidity and log vapour pressure is small.

2.3 Effect of spatial resolution

Geophysical fields usually show a certain continuity, that is variables do not change much on small spatial or temporal scales. On larger scales (larger than the autocorrelation scale of the quantity in question) we expect larger variations of the fields since the probability that we relate quantities in two different air–masses (air–masses of different origin, e.g. of tropical and polar origin) increases with the scale of our investigation. Therefore we expect that the width of the distributions for fluctuations increases with the spatial scale of the analysis. This is confirmed by the data presented in Fig. 2a,b. These reveal how the fluctuation distributions of temperature and relative humidity depend on the underlying spatial resolution. We have compared T42 with T21, T30, and T63 resolutions, corresponding to grid sizes from 208 km (T63) to 625 km (T21) at the equator.

Table 2 shows the variation of the statistical measures with spatial resolution in numbers. As expected, the measures of width (standard deviation and variance) decrease with increasing resolution. The skewness behaves differently for temperature and relative humidity, respectively; its variation with resolution is weak. The values of kurtosis increase strongly with increasing resolution, quantifying the increasingly steeper distribution tails. This result is unexpected. It implies that the fluctuation statistics differ increasingly from a Gaussian distribution for finer

spatial resolutions, at least up to T63 resolution. This surprising result will be explained in Part 2 of our paper.

2.4 Dependence of moments on grid box mean of RH_i

To show how the distribution of fluctuations of relative humidity varies with the mean relative humidity over ice, we binned the respective fluctuation data in T42 resolution into classes 10% wide in RH_i, with bins centred at 10%, 20%, 30%, ... The resulting low order moments from Eqs. (1-3) in Table 3 show several interesting features. The widest distributions are those with mean RH_i in a medium range (say, 50 to 120%); the distributions with either rather dry or rather moist (i.e. more extreme) mean values are narrower. "Dry" distributions are positively skewed, and "moist" distributions are negatively skewed. Distributions are close to symmetric when the mean RH_i is about 70 to 80%.

The dependence of skewness on the mean RH_i in Fig. 3 shows individual values of skewness to reach considerable magnitudes. The skewness found before for the overall distribution of δRH_i must therefore be considered merely a random value; it depends on the relative frequency of mean RH_i values in the data set:

$$S = \sum_{c=1}^{C} \frac{N_c}{N} S_c, \tag{4}$$

where N_c is the number of observations in humidity class c, and S_c is the skewness taken for that class. The ratio N_c/N is the weight applied to class c in the overall skewness. Since nearly saturated and supersaturated cases occur less frequently in the upper troposphere than drier and moderately moist cases (GIERENS etal., 1999; SPICHTINGER etal., 2002), the positive skewness values for the latter dominate in the overall data, which explains the occurrence of significant positive skewness in the overall distribution of fluctuations of relative humidity. Notably, the skewness stays more or less constant in the RH_i–classes beyond 100%. The kurtosis decreases non–monotonically from extremely high values at the low humidity end to about zero at the very moist end of the humidity range considered. Further, Table 3 shows that a statistically significant positive kurtosis in the overall distribution is not an incidental result. Except from the extremely moist cases, all distributions of fluctuations of RH_i are more or less sharply peaked at $\delta RH_i = 0$.

2.5 Geographical variation of standard deviations

So far we have looked at the data regardless of their geographical position. Here we show how the widths of the fluctuation distributions vary with their location on the globe. For that purpose we combine all fluctuation data for a given grid cell and compute from these a mean variance for that cell. Only cells with at least 160 data points are retained in the analysis, in order to secure a good statistical ensemble. From the mean variances we compute the mean standard deviations (by taking the square root) that are presented in Figs. 4, 5, and 6.

Figs. 4–6 display a contrast between tropics and mid–latitudes (only the northern hemisphere mid–latitudes are covered by MOZAIC). For instance, the temperature fluctuations tend to be small in the tropics and larger in the mid–latitudes, while fluctuations of log water vapour partial pressure and relative humidity are larger in the tropics than in mid-latitudes. The large fluctuations of the water vapour variables in the tropics is certainly caused by deep convection, which is a small scale phenomenon relative to T42 resolution. Deep convection is the main source of water vapour in the considered altitude range in the tropics, but it occurs in a random (intermittent) fashion. The humidity fluctuations also show a tendency to smaller values at higher altitude, consistent with the distributions shown in Figs. 1b,c. Temperature fluctuations are larger in the extra–tropics than in the tropics. One component contributing to the larger T–fluctuations in the extra–tropics might be simply the large north–south temperature gradient in the vicinity of the jet stream, which implies temperature variations in the respective grid cells even without other sources. Other origins of large temperature fluctuations in the extra–tropics are fronts and tropopause folds, and waves emanated from the jet stream (SPICHTINGER etal., 2005). Orographic waves could in principle excite temperature fluctuations as well in the tropics as in extra–tropics, but the vagaries of continental drift have placed more mountainous regions in the northern hemisphere mid–latitudes. Hence, orographic waves contribute to temperature fluctuations more in the latter regions than in the tropics. On the map of temperature fluctuations one may also notice a certain land–sea contrast, especially between North America and the Atlantic ocean, and between Europe and the Atlantic. This is also probably due to orographic excitation.

2.6 Bivariate p.d.f. of δT and δRH_i

Fig. 7 shows non–normalised bivariate p.d.f.s for joint fluctuations of temperature and relative humidity with respect to ice at T42 resolution. As shown by GIERENS etal. (1997), the shape of the bivariate p.d.f. depends on the respective mean phase state. This becomes evident from the bivariate p.d.f.s for the mean states

- $(T = -53.5 \pm 0.5°\text{C}, RH_i = 70 \pm 5\%)$ in Fig. 7a,
- $(T = -53.5 \pm 0.5°\text{C}, RH_i = 100 \pm 5\%)$ in Fig. 7b, and
- $(T = -53.5 \pm 0.5°\text{C}, RH_i = 130 \pm 5\%)$ in Fig. 7c.

The temperature range $T = -53.5 \pm 0.5°\text{C}$ has been chosen because it contains the largest number of data in our data base.

Apart from the zero–axes, the panels in Fig. 7 contain lines that represent the derivative dRH_i/dT at the respective mean phase state. Pure fluctuations in temperature lead to fluctuations in RH_i along this line, whereas pure fluctuations in vapour pressure lead to fluctuations in RH_i along the vertical line.

All bivariate p.d.f.s have an approximately oval shape that is extended in the direction of the respective derivative. In order to see whether fluctuations of T or e dominate those of RH_i we consider the total differential of RH_i:

$$dRH_i = \frac{\partial RH_i}{\partial T}\, dT + \frac{\partial RH_i}{\partial e}\, de = -RH_i \frac{L}{R_v}\frac{dT}{T^2} + RH_i \frac{de}{e}.$$

Hence we have for the relative fluctuations of relative humidity

$$\frac{dRH_i}{RH_i} = -\frac{L}{R_v}\frac{dT}{T^2} + \frac{de}{e}.$$

We now form the ratio R, viz.

$$R := \frac{R_v}{L}\, T^2\, \frac{\sigma_{\delta e/e}}{\sigma_{\delta T}} = 1.72 \times 10^{-4} \left(\frac{T}{\text{K}}\right)^2 \frac{\sigma_{\delta e/e}}{\sigma_{\delta T}}.$$

R can be interpreted as the influence ratio of vapour concentration to temperature fluctuations in controlling instantaneous fluctuations of relative humidity. For the conditions from Table 1 and with a typical temperature of 220 K in the upper troposphere this ratio is about 2. It seems plausible to assume that neither $\sigma_{\delta T}$ nor $\sigma_{\delta e/e}$ will vary much in the free troposphere. Then, $R \propto T^2$, that is, R increases with decreasing altitude. From 200 to 270 K, R varies between

1.6 and 2.9. In other words, fluctuations of vapour pressure generally have a larger influence on fluctuations of relative humidity than temperature fluctuations, in particular in the lower layers of the free troposphere. However, the influence of temperature fluctuations is not negligible, in particular in the upper troposphere. Thus both should be taken into account in a statistical cloud scheme for cirrus clouds, all the more as it is the temperature fluctuations that eventually control the number density of ice crystals.

While GIERENS etal. (1997) modelled the bivariate p.d.f. by fitting Lorentz distributions (also known as Cauchy distributions) to the 1–d distributions of the fluctuations, we will not do this here because the tails of the distributions differ too much from Lorentzians. Instead we will discuss potential causes for the found peculiar distributions in Part 2.

3 Discussion

The present work was initiated with the main goal to provide data on instantaneous fluctuations of the geophysical fields relevant for cloud formation to be used in future stochastic cloud modules for large–scale models, e.g. for weather prediction or climate research. For this purpose, it is sufficient to derive the bivariate p.d.f.s of the fluctuations, because these are used to compute the overlap integrals which measure how much of the fluctuations reach into that part of the $\{T, RH_i\}$ phase space where cloud formation takes place. Unfortunately, a single flight through a single grid box gives only very limited information on the then present fluctuations within that grid volume. This is the problem of representativeness that is also an issue for radiosonde measurements, for instance. Satellite data suffer from low resolution, and campaign data suffer from their sparseness, which is another kind of representativeness problem. Hence we think that MOZAIC data is the best available compromise, at least for studying the overall statistics of fluctuations, their geographical and seasonal variation, etc. For this kind of study, it has better representativeness than radiosondes, better spatial resolution than satellite data, and covers a larger part of the globe than campaign data. Furthermore, MOZAIC aircraft have been carrying the same instrumentation since more than ten years, implying a more homogeneous dataset than obtainable with a collection of campaign data. However, the distribution of fluctuations in a certain situation (i.e. in a certain grid volume at a given time) can probably not be studied in sufficient detail and for a sufficiently wide variety of situations from observation data alone; we can perhaps obtain excellent snapshots using campaign data but not more. Fur such a

purpose it seems necessary to use cloud resolving modelling (e.g. TOMPKINS, 2002), as far as possible validated with observation data. The MOZAIC data as shown in the present paper can be useful for such a validation purpose.

TOMPKINS (2002) gives an overview of various cloud cover parameterisations, including so–called statistical schemes. These schemes often use a quantity s that combines fluctuations of the total water mixing ratio (i.e. water in all its phases), q'_{tot}, and of temperature T'. If the statistics of both these quantities and their correlation were known from measurements or from cloud–resolving model simulations, the distribution of s could be obtained as a convolution of the distributions for q'_{tot} and T'. Unfortunately, the required data are difficult to obtain; hence all approaches generally make assumptions either directly on the distribution of s or on the distribution of q'_{tot}, ignoring the temperature variations (TOMPKINS, 2003). The MOZAIC data in principle offer the possibility to check such assumptions. For example, we have seen that temperature fluctuations should not be neglected in a statistical cloud scheme, in particular for the cirrus clouds in the upper troposphere.

One has to be cautious when comparing a model distribution of fluctuations at a certain location and a certain time step with averaged data like those presented here. An illustrative example is bimodality. We have tested whether bimodality shows up in grid boxes where the MOZAIC air–plane changes from troposphere to stratosphere or vice versa (determined by the ozone mixing ratio). In order to avoid smoothing effects as much as possible only grid boxes with an equal number of tropospheric and stratospheric points were retained. We checked fluctuations of temperature and relative humidity. Surprisingly, the distributions constrained to those grid boxes show no bimodality, they are still peaked at zero, although the peak is not as sharp as in the overall distribution. The constrained distributions are broader than the overall distributions reflecting the change of airmass, and their kurtosis values are lower, reflecting the reduced sharpness of the peak. When we looked closer to the data and considered the single cases (i.e. one flight through one grid box) the bimodality was present; the averaging smoothes it out. This again stresses the point that averaged data like those presented here cannot be directly employed for a statistical cloud scheme; they may rather be used for validation.

It is known that humidity fluctuations occur on very small scales, much smaller than the resolution of the MOZAIC data (which is evident from the small scales of non–stratus clouds). Hence the question arises how fluctuations on scales smaller than the 15 km resolution of MOZAIC would contribute to the distributions if one could measure them with MOZAIC. For-

tunately, water vapour measurements with very high frequency (20 Hz) have been used by CHO etal. (2000) to determine structure functions. It turned out that water vapour exhibits (anomalous) scaling (i.e. behaves self–similarly) on scales larger than 43 m in their data. The second structure function has an exponent of approximately 2/3 in the free troposphere; it is dual to a power spectrum $E(k) \propto k^{-5/3}$. The total "energy" is equivalent to the variance in the underlying data. Integrating the power spectrum a) from $k = 1/300$ km^{-1} to $k = 1/15$ km^{-1} (i.e. from the T42 grid size to the MOZAIC resolution) and b) from $k = 1/300$ km^{-1} to $k = 1$ km^{-1} (i.e. to a much finer resolution) and taking the ratio gives 1.13 (integrating case b up to $k = \infty$ gives 1.16). Hence we may conclude that the variance of the water vapour fluctuation distributions as seen by the MOZAIC measurements is perhaps underestimated by about 15%.

For the present purpose it was irrelevant to use the information on the *sequence* of the MOZAIC data. Yet, they may also be considered as time series, i.e. stochastic processes. Then the sequence of the data is the prime interest. In such an approach one can obtain important information on autocorrelation lengths (the scale at which the autocorrelation function drops below a certain threshold, usually zero), structure functions and scaling behaviour (PIERREHUMBERT, 1996; CHO etal., 2000), and (multifractal) characterisations of non–stationarity and intermittency (e.g. DAVIS etal., 1994; SORNETTE, 2004). Such topics will be treated in Part 2.

4 Summary

We have investigated statistics of instantaneous fluctuations of temperature, vapour pressure, and relative humidity using nine years of MOZAIC data, which gave about 5 million usable data points. This study has been undertaken with the idea that such data can be used for validation of statistical cloud schemes.

It turned out that the probability density distributions are peaked, and clearly non–Gaussian. Whereas the p.d.f. of vapour pressure fluctuations shows convex wings, the two other p.d.f.s display an ogival shape, in particular the p.d.f. of humidity fluctuations. Low order statistical moments (up to kurtosis) have been determined, and the influence of spatial resolution on the moments has been studied. In particular the widths of the distributions turn out to shrink with higher resolution. A Gaussian shape of the p.d.f.s did not appear. The skewness of the p.d.f.s of relative humidity, conditioned on the mean relative humidity, depends on the latter. The p.d.f. is close to symmetric when the background humidity is approximately 70%. The distributions

are right skewed for drier and left skewed for moister backgrounds.

Seasonal variation of the distributions were studied and appeared as weak. Geographical distributions of the mean standard deviations of the fluctuations were shown. It turned out that temperature fluctuations are larger in the extra–tropics and over land than over the tropics and over the ocean. On the contrary, humidity variations (absolute and relative) are largest were deep convection serves as the dominant source of moisture in the main flight altitudes, that is in the tropics, in particular over the continents.

From our results we conclude that temperature variations cannot be neglected in a statistical cloud scheme. Bivariate distributions for joint fluctuations of temperature and relative humidity demonstrate the dominating influence of temperature variations on fluctuations of relative humidity except for supersaturated background states where fluctuations of vapour pressure become equally influencing.

The peculiar ogival shape of the humidity p.d.f.s have been found also in studies on turbulence and other phenomena. In turbulence, the ogival shape is related to intermittency which can be demonstrated using results from a numerical simulation of Rayleigh–Bénard convection. These and other investigations detailing the cause of the ogival shape will be presented in Part 2.

Acknowledgments

Fruitful discussions with Bernd Kärcher are gratefully acknowledged. Two reviewers provided useful comments that led to considerable improvement of the paper. MOZAIC (www.fz-juelich.de/icg/icg-ii/mozaic/) has been sponsored since 1994 by the Commission of the European Communities under Framework Programmes 4, 5, and 6. This work contributes to the DLR/HGF–project “Particles and Cirrus Clouds” (PAZI–2).

References

BORTZ, S.E., M.J. PRATHER, J.-P. CAMMAS, V. THOURET, H. SMIT, 2006: Ozone, water vapor, and temperature in the upper tropical troposphere: Variations over a decade of MOZAIC measurements. – J. Geophys. Res. **111**, D05305, doi:10.1029/2005JD006512.

CHO, J.Y.N., R.E. NEWELL, G.W. SACHSE, 2000: Anomalous scaling of mesoscale tropospheric humidity fluctuations. – Geophys. Res. Lett. **27**, 377–370.

DAVIS, A., A. MARSHAK, W. WISCOMBE, R. CAHALAN, 1994: Multifractal characterizations of nonstationarity and intermittency in geophysical fields: Observed, retrieved, or simulated. – J. Geophys. Res. **99**, 8055–8072.

DOTZEK, N., K. GIERENS, H.G.J. SMIT, 2006: Instantaneous fluctuations of temperature and moisture in the upper troposphere and tropopause region. Part 2: Structure functions and intermittency. – Meteorol. Z., in preparation.

GIERENS, K.M., U. SCHUMANN, H.G.J. SMIT, M. HELTEN, G. ZÄNGL, 1997: Determination of humidity and temperature fluctuations based on MOZAIC data and parametrization of persistent contrail coverage for general circulation models. – Ann. Geophys. **15**, 1057–1066.

GIERENS, K., U. SCHUMANN, M. HELTEN, H.G.J. SMIT, A. MARENCO, 1999: A distribution law for relative humidity in the upper troposphere and lower stratosphere derived from three years of MOZAIC measurements. – Ann. Geophys. **17**, 1218–1226.

HELTEN, M., H.G.J. SMIT, W. STRÄTER, D. KLEY, P. NEDELEC, M. ZÖGER, R. BUSEN, 1998: Calibration and performance of automatic compact instrumentation for the measurement of relative humidity from passenger aircraft. – J. Geophys. Res. **103**, 25 643–25 652.

HELTEN, M., H.G.J. SMIT, D. KLEY, J. OVARLEZ, H. SCHLAGER, R. BAUMANN, U. SCHUMANN, P. NEDELEC, A. MARENCO, 1999: In–flight intercomparison of MOZAIC and POLINAT water vapor measurements. – J. Geophys. Res. **104**, 26 087–26 096.

MARENCO, A., V. THOURET, P. NEDELEC, H. SMIT, M. HELTEN, D. KLEY, F. KARCHER, P. SIMON, K. LAW, J. PYLE, G. POSCHMANN, R. VON WREDE, C. HUME, T. COOK, 1998: Measurement of ozone and water vapor by Airbus in–service aircraft: The MOZAIC airborne program, an overview. – J. Geophys. Res. **103**, 25 631–25 642.

PIERREHUMBERT, R.T., 1996: Anomalous scaling of high cloud variability in the tropical Pacific. – Geophys. Res. Lett. **23**, 1095–1098.

SORNETTE, D., 2004: Critical Phenomena in Natural Sciences, 2nd ed. – Springer Verlag, Berlin, 528 pp.

SPICHTINGER, P., K. GIERENS, W. READ, 2002: The statistical distribution law of relative humidity in the global tropopause region. – Meteorol. Z. **11**, 83–88.

SPICHTINGER, P., K. GIERENS, A. DÖRNBRACK, 2005: Formation of ice supersaturation by mesoscale gravity waves. – Atmos. Chem. Phys. **5**, 1243–1255.

TOMPKINS, A.M., 2002: A prognostic parameterization for the subgrid–scale variability of water vapor and clouds in large–scale models and its use to diagnose cloud cover. – J. Atmos. Sci. **59**, 1917–1942.

TOMPKINS, A.M., 2003: Impact of temperature and humidity variability on cloud cover assessed using aircraft data. – Q. J. R. Meteorol. Soc. **129**, 2151–2170.

Tables

Table 1: Statistical description of the distributions of instantaneous fluctuations of temperature, relative humidity over ice, water vapour partial pressure and the relative fluctuations of water vapour partial pressure in T42 resolution. The low order moments are also given for northern winter (DJF) and summer (JJA) months.

variable	σ	variance	skewness	kurtosis
δT	0.82	0.68	0.24	7.64
δRH_i	9.57	91.7	0.23	8.16
δe	0.61	0.37	1.36	120
$\delta e/e$	0.18	0.03	1.71	24.4
DJF				
δT	0.83	0.69	0.21	6.87
δRH_i	8.44	71.2	0.26	10.6
$\delta e/e$	0.16	0.03	1.43	18.8
JJA				
δT	0.82	0.67	0.27	9.20
δRH_i	10.7	115	0.22	6.82
$\delta e/e$	0.20	0.04	1.78	23.7

Table 2: Dependence of standard deviation, variance, skewness and kurtosis of fluctuations of temperature and relative humidity over ice on spatial resolution.

δT (K)	σ	variance	skewness	kurtosis
T21	1.20	1.44	0.15	5.42
T30	0.95	0.91	0.20	6.60
T42	0.82	0.68	0.24	7.64
T63	0.70	0.49	0.33	10.6
δRH_i (%)	σ	variance	skewness	kurtosis
T21	12.96	168	0.25	5.23
T30	10.80	117	0.25	6.89
T42	9.57	91.7	0.23	8.16
T63	5.51	30.4	0.49	17.7
δe (Pa)	σ	variance	skewness	kurtosis
T21	0.61	0.37	1.36	120
T30	0.65	0.42	1.46	107
T42	0.61	0.37	1.36	120
T63	0.44	0.20	2.09	145

Table 3: Standard deviation, variance, skewness and kurtosis of fluctuations of RH_i in T42 resolution as a function of the respective mean RH_i.

RH_i (%)	σ	variance	skewness	kurtosis
10	2.21	4.90	3.06	55.5
20	3.89	15.1	2.69	36.1
30	6.46	41.8	1.91	16.5
40	9.09	82.6	1.39	9.40
50	11.4	131	0.90	5.45
60	13.0	169	0.53	3.64
70	13.9	194	0.21	2.77
80	13.9	192	-0.09	2.77
90	13.2	174	-0.32	3.02
100	12.2	148	-0.50	3.84
110	11.0	121	-0.71	4.83
120	10.2	104	-0.71	4.70
130	9.58	91.7	-0.80	5.36
140	8.73	76.2	-0.73	4.84
150	8.05	64.9	-0.63	3.34
160	6.85	47.0	-0.66	2.76
170	5.68	32.3	-0.82	2.81
180	4.49	20.2	-0.76	1.26

Figure captions

Figure 1: P.d.f.s of MOZAIC instantaneous fluctuations of (a) temperature, (b) water vapour pressure, and (c) relative humidity over ice in T42 resolution, from two layers in the tropopause region, $275 \geq p \geq 225$ hPa (dashed) and $225 \geq p \geq 175$ hPa (solid).

Figure 2: P.d.f.s of MOZAIC instantaneous fluctuations of (a) temperature, (b) RH_i in the tropospause region (275 to 175 hPa) for T21, T30, T42, and T63 spatial resolutions.

Figure 3: Skewness of the MOZAIC RH_i fluctuations in T42 resolution as a function of grid box mean relative humidity over ice, $\overline{RH_i}$. Values from Table 3.

Figure 4: Map of geographical variation of the standard variation, σ_T, of temperature fluctuations on the T42 grid. Upper panel: Pressure range 175 to 225 hPa, lower panel: 225 to 275 hPa.

Figure 5: As Fig. 4, but for $\sigma_{\delta e/e}$.

Figure 6: As Fig. 4, but for σ_{RH_i}.

Figure 7: Non–normalised bivariate p.d.f.s of MOZAIC joint fluctuations of temperature and relative humidity over ice in T42 resolution for the pressure range 275 to 175 hPa. The mean states have temperature $T = -53.5 \pm 0.5$°C and relative humidity (a) $RH_i = 70 \pm 5\%$, (b) $RH_i = 100 \pm 5\%$, (c) $RH_i = 130 \pm 5\%$. Contours (shading) are 1, 3, 10, and 30 samples. The slant line represents the derivative dRH_i/dT at the mean state.

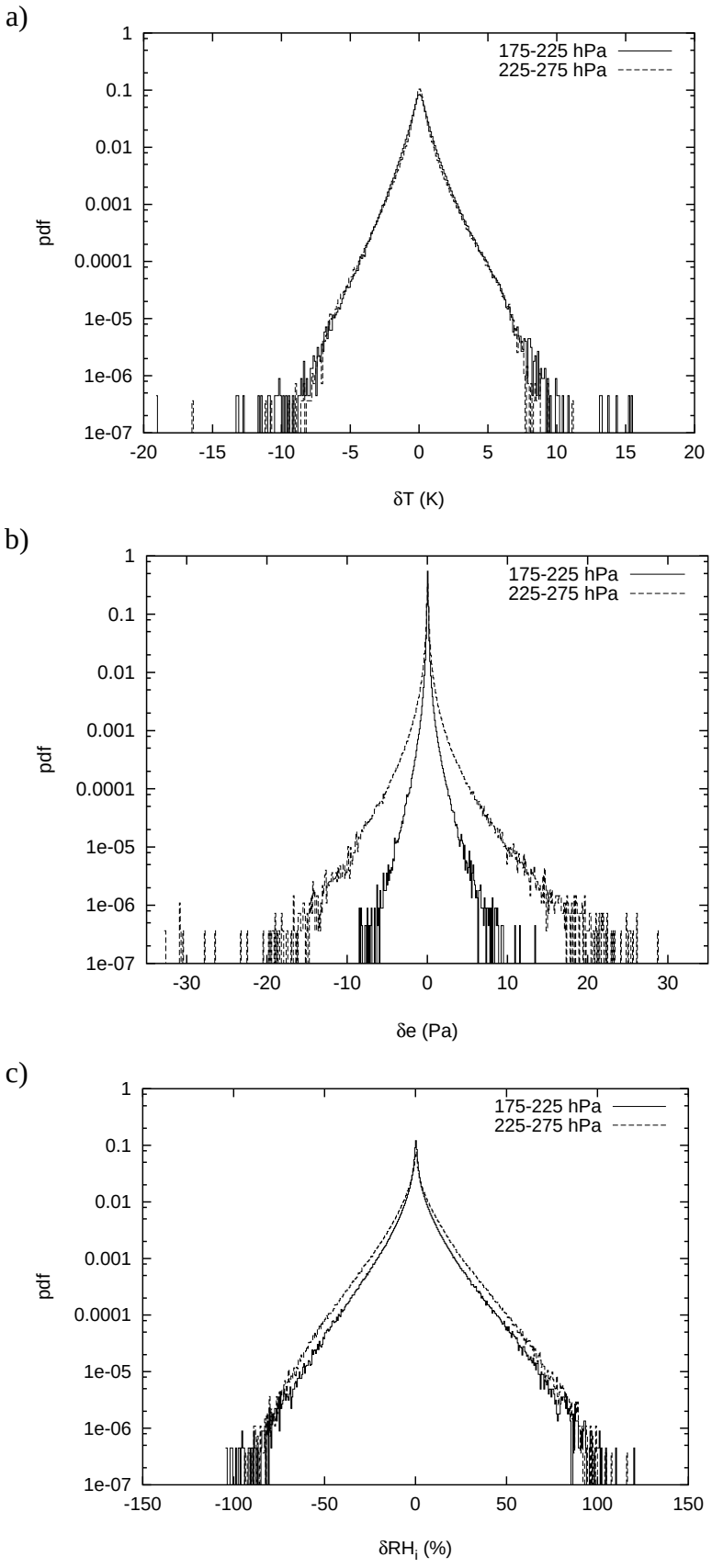

Figure 1: P.d.f.s of MOZAIC instantaneous fluctuations of (a) temperature, (b) water vapour pressure, and (c) relative humidity over ice in T42 resolution, from two layers in the tropopause region, $275 \geq p \geq 225$ hPa (dashed) and $225 \geq p \geq 175$ hPa (solid).

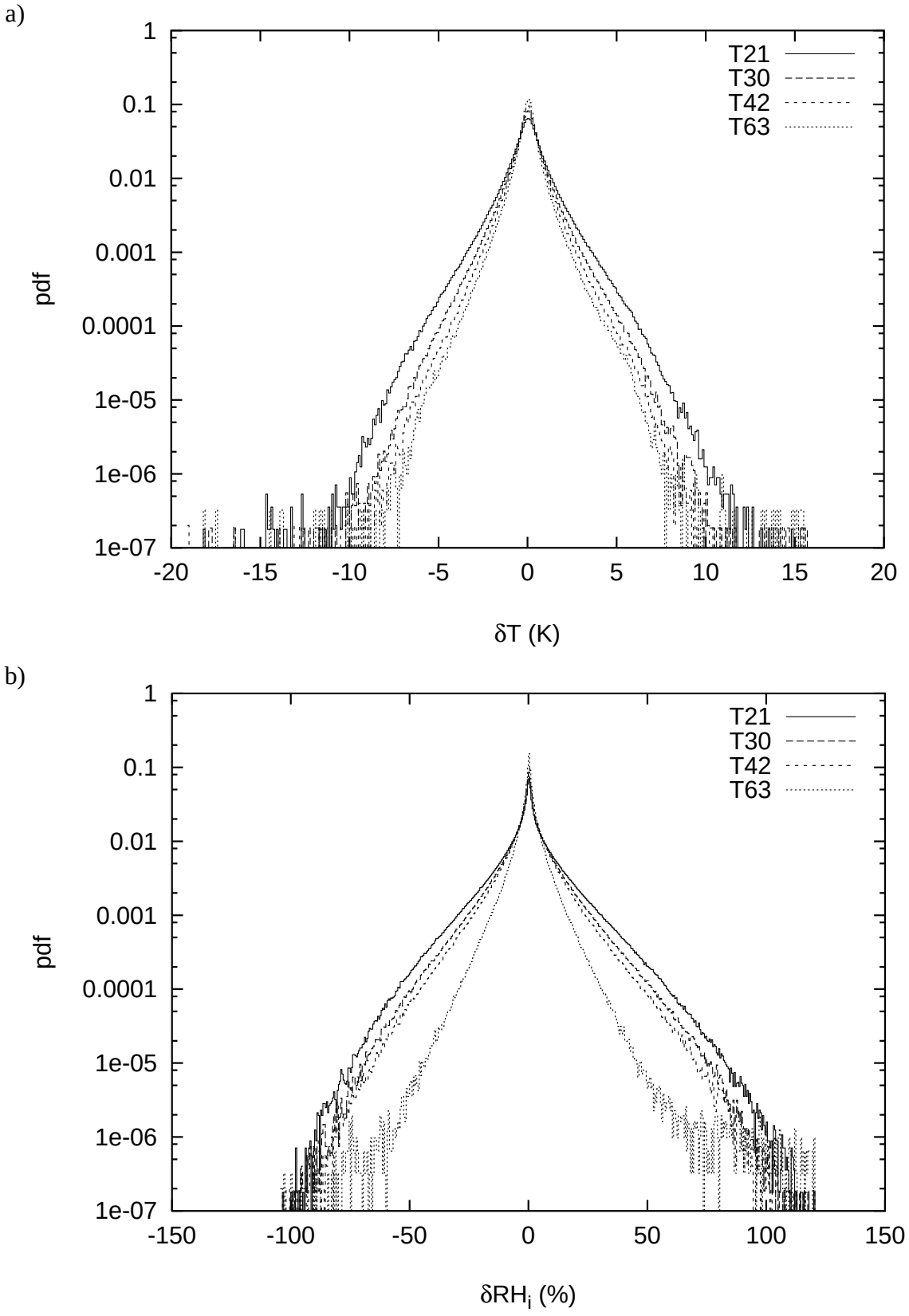

Figure 2: P.d.f.s of MOZAIC instantaneous fluctuations of (a) temperature, (b) RH_i in the tropospause region (275 to 175 hPa) for T21, T30, T42, and T63 spatial resolutions.

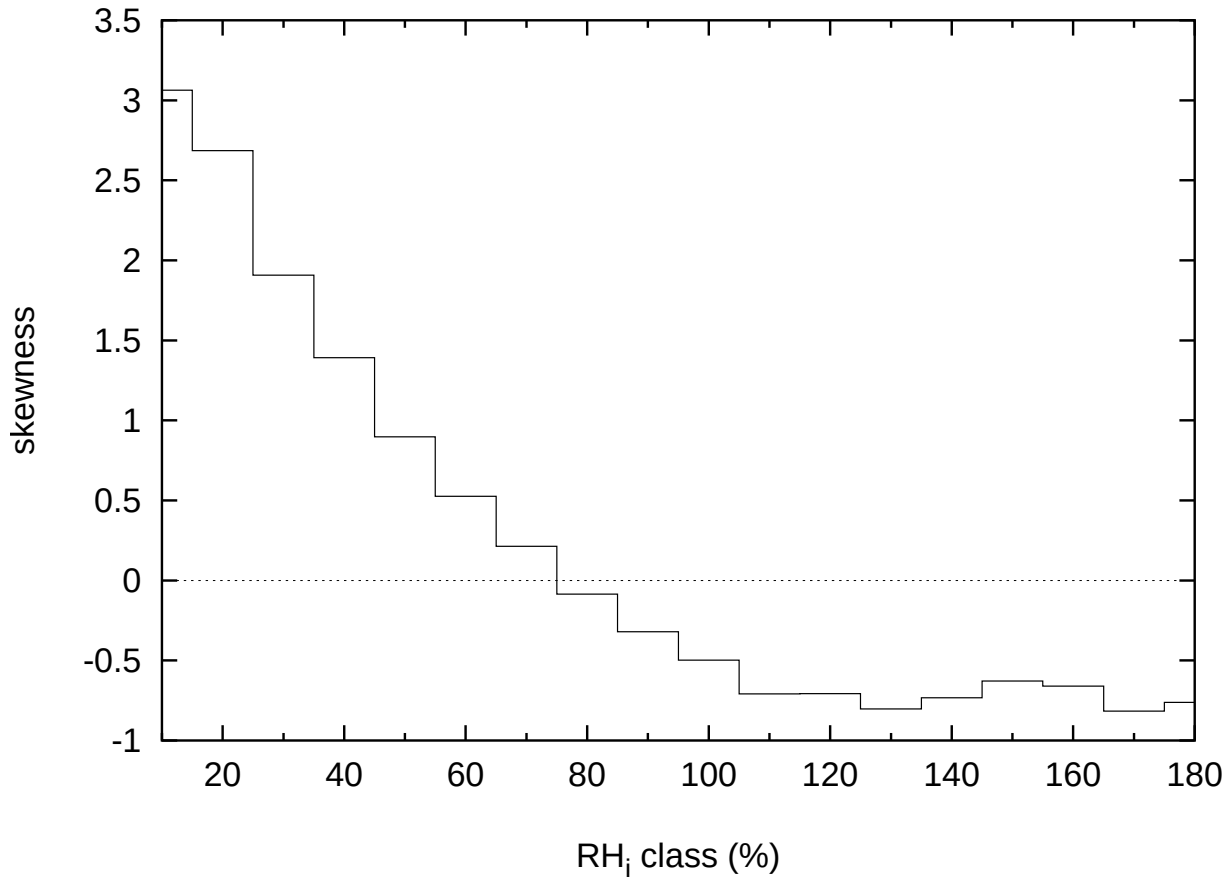

Figure 3: Skewness of the MOZAIC RH_i fluctuations in T42 resolution as a function of grid box mean relative humidity over ice, $\overline{RH_i}$. Values from Table 3.

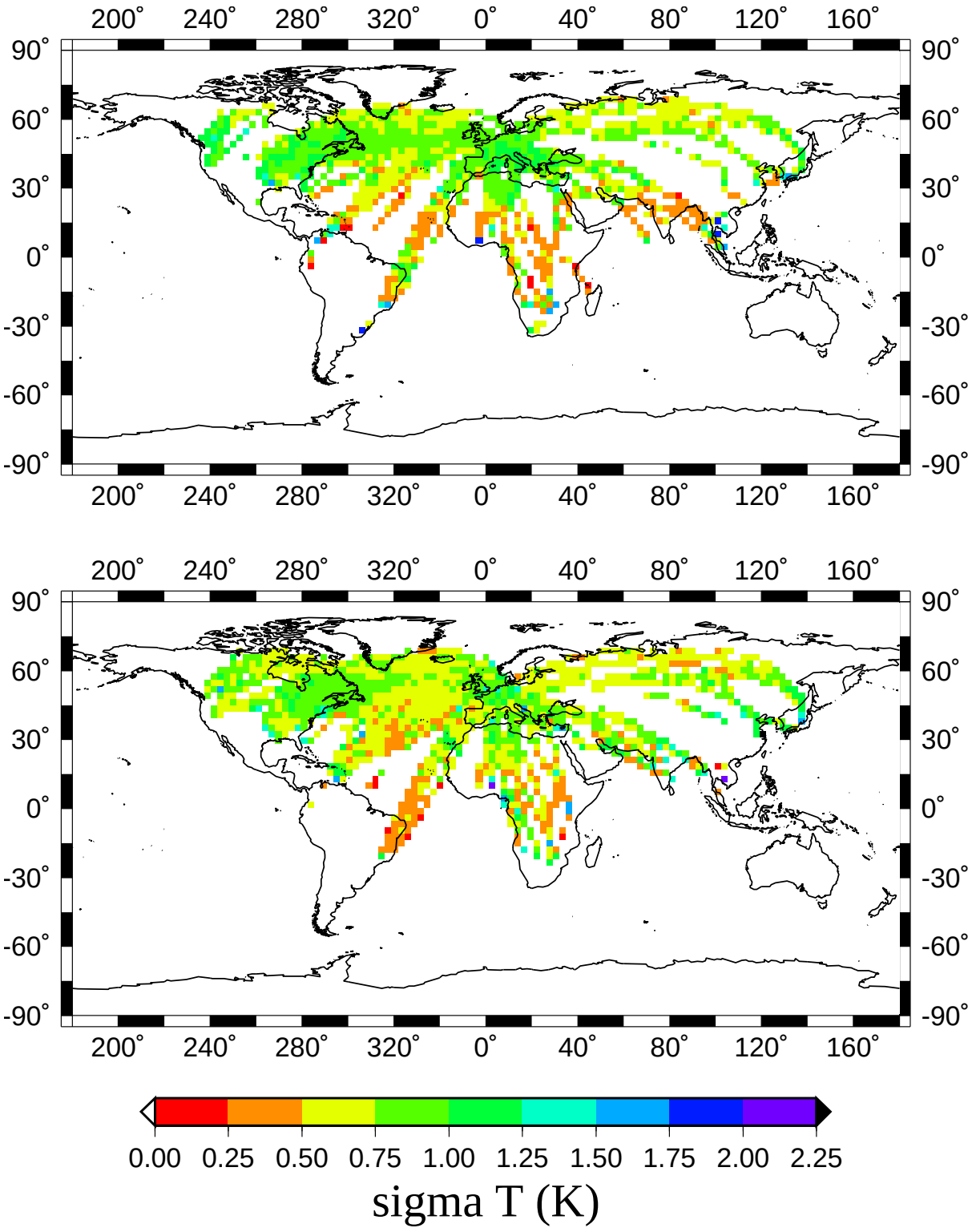

Figure 4: Map of geographical variation of the standard variation, σ_T, of temperature fluctuations on the T42 grid. Upper panel: Pressure range 175 to 225 hPa, lower panel: 225 to 275 hPa.

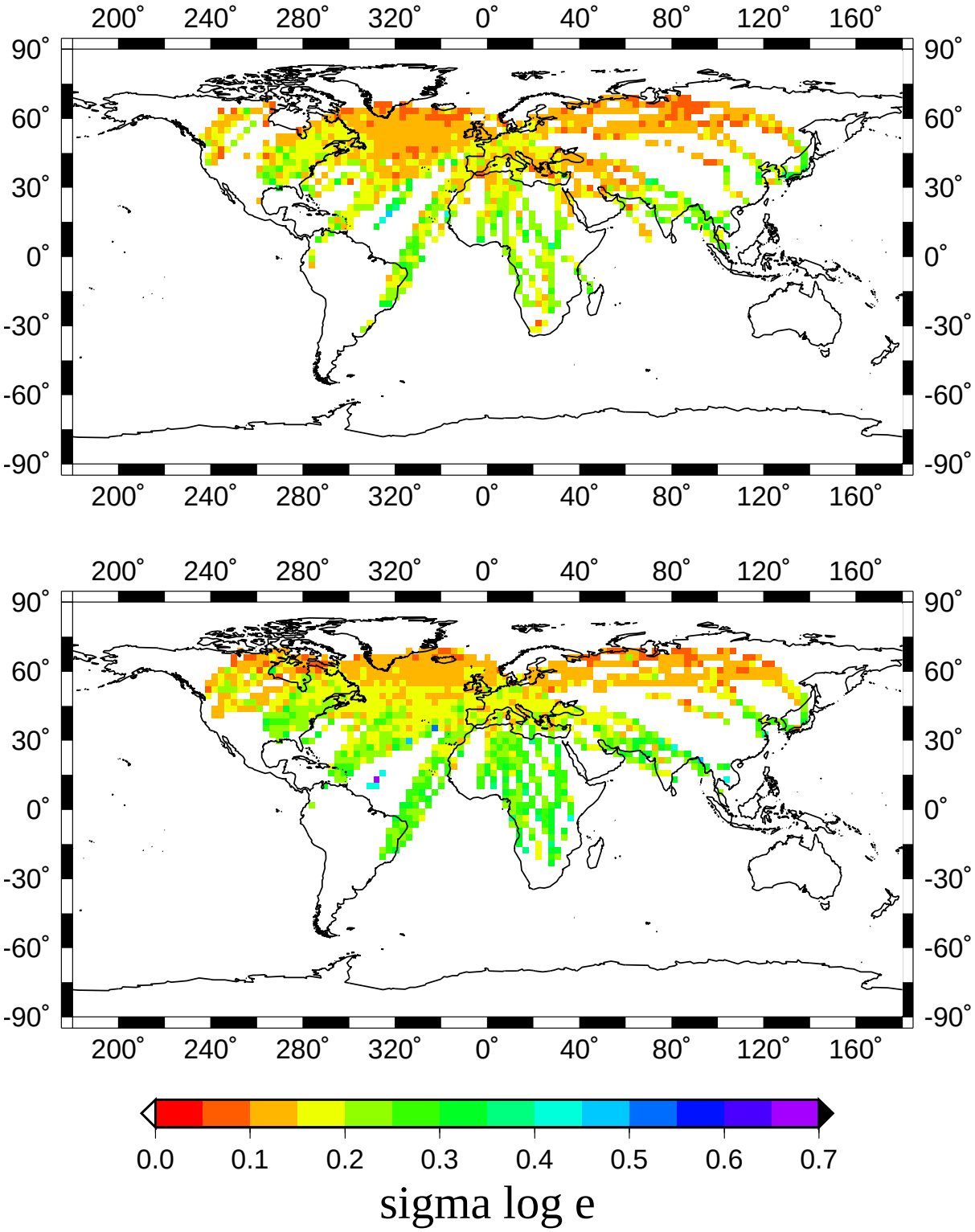

Figure 5: As Fig. 4, but for $\sigma_{\delta e/e}$.

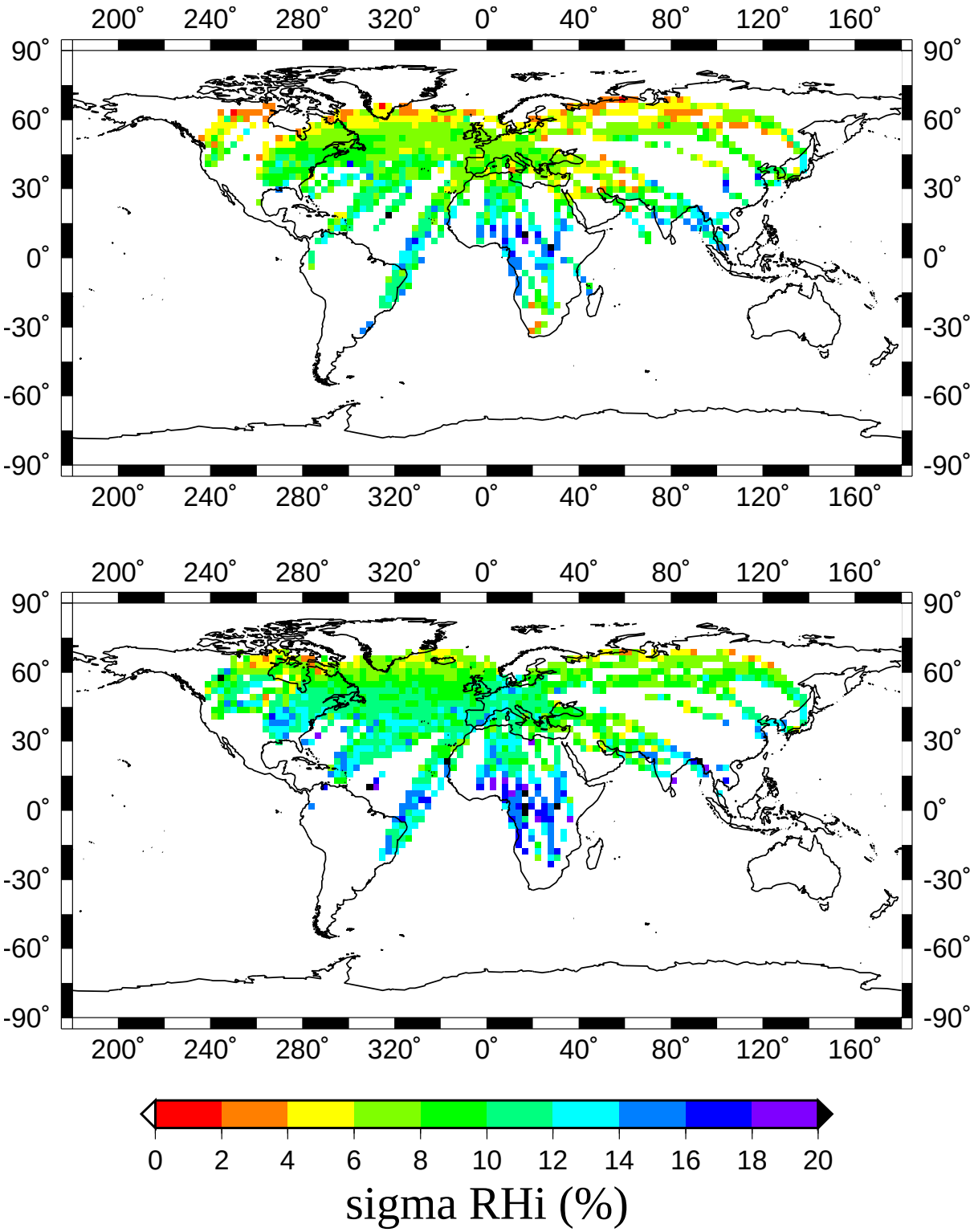

Figure 6: As Fig. 4, but for σ_{RH_i}.

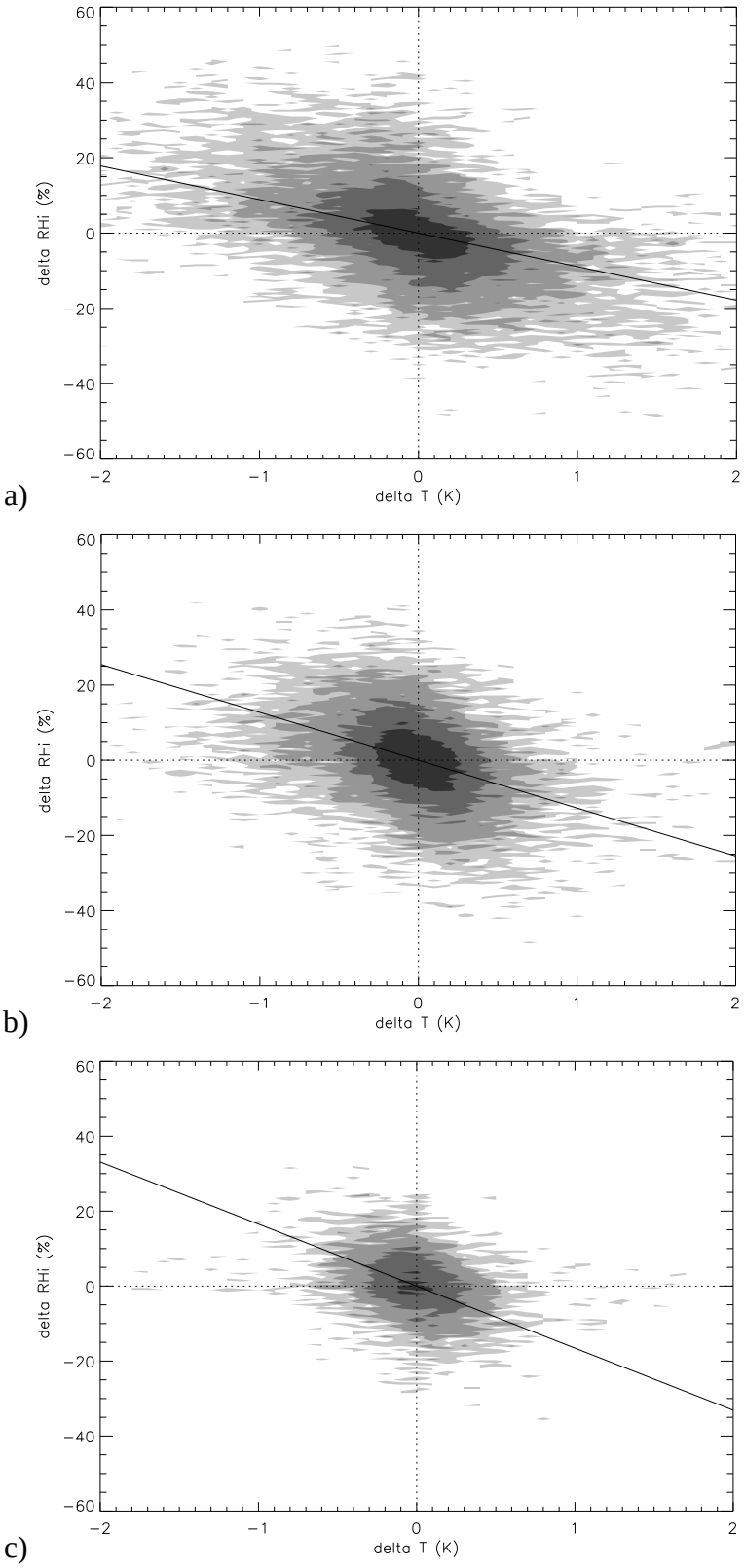

Figure 7: Non–normalised bivariate p.d.f.s of MOZAIC joint fluctuations of temperature and relative humidity over ice in T42 resolution for the pressure range 275 to 175 hPa. The mean states have temperature $T = -53.5 \pm 0.5$°C and relative humidity (a) $RH_i = 70 \pm 5\%$, (b) $RH_i = 100 \pm 5\%$, (c) $RH_i = 130 \pm 5\%$. Contours (shading) are 1, 3, 10, and 30 samples. The slant line represents the derivative dRH_i/dT at the mean state.